ISSN 1330-3651(Print), ISSN 1848-6339 (Online)
https://doi.org/10.17559/TV-20231011001015
Original scientific paper

Advanced Optical Coherence Tomography for Real-Time Detection of Defects in Aluminum Alloy Laser Welding

Zhengying JIANG, Zhengang JIANG*

Abstract: In order to measure the quality of aluminum alloy laser welding workpiece online, an optical coherence tomography on-line detection system was established. Porosity is one of the most common defects in laser welding of aluminum alloy. The porosity produced during welding will seriously affect the welding quality. Firstly, a test device of laser welding quality detection system is built based on optical coherence tomography algorithm. Then, the theoretical model of the optical coherence tomography detection system is built, and the key parameters affecting the detection device are qualitatively analyzed. Then, deep convolutional neural network algorithm is used to process the image. Finally, the testing equipment is used to test the sample, and the testing results are analyzed. The experimental results show that this method can detect the weld quality of laser welding, and the detection accuracy is 20 μm.

Keywords: deep convolutional neural network; laser welding; optical coherence tomography

1 INTRODUCTION

In recent years, the field of laser processing, encompassing laser welding, laser additive manufacturing, and laser material reduction manufacturing, has witnessed remarkable advancements. Characterized by high processing quality, efficiency, and non-contact nature, these technologies have found extensive applications in sectors such as automotive, aerospace, and electronic information. The evolution of these industries has concurrently escalated the demand for precision in laser processing. However, challenges such as particle eruption during processing often lead to defects like porosity and cracks on the workpiece. Consequently, the accurate, real-time identification, monitoring, and control of welding quality have emerged as pivotal areas of research. The scholarly community has extensively explored laser processing monitoring and quality control, employing various signals like light, sound, heat, and electricity. These studies aim to establish a direct correlation between processing signals and outcomes, thereby facilitating control over the processing parameters. However, achieving precise, controllable results often necessitates complex models, which can be challenging to implement widely due to their complexity and lack of demonstrability. Optical Coherence Tomography (OCT), a non-destructive, non-contact, high-resolution 3D imaging technology, stands out with its high signal-to-noise ratio, rapid imaging capabilities, and minimal sensitivity degradation with depth. Its applications span across diverse fields, including skin detection, ophthalmic imaging, medical endoscopy, and angiography. This paper delves into the application of OCT in analyzing laser welding quality. OCT's ability to measure laser weld depth and profile in real-time, coupled with its micron-level accuracy, makes it an invaluable tool for process monitoring and quality assurance in laser welding [1-4]. In the realm of online weld depth measurement for deep penetration laser welding, significant strides have been made. Mayr, A et al.'s research on a quality monitoring system using machine learning techniques for predicting weld defects and overall quality, and Schaumber, K et al.'s exploration of thermal imaging in laser welding of copper components, are notable contributions. Similarly, Boley, M. et al.'s study on the dynamics of high-speed X-ray imaging systems in laser processing has provided valuable insights for online monitoring and closed-loop control of laser processing [5-7]. The growing demand for online process monitoring in welding technology underscores the need for advanced solutions like OCT, which offers highly accurate surface topography measurements at a temporal resolution of up to several thousand Hertz, unaffected by radiation interference during welding. Recent advancements in image processing chips have opened new avenues for integrating artificial intelligence algorithms into laser processing. Researchers like Christian Stadter et al. have pioneered in establishing analysis models for weld depth and surface processing quality using machine learning methods. Their work in analyzing the data processing neural network model for the welding process of galvanized steel plates using OCT technology is a testament to the potential of well-trained neural network models in predicting the surface quality of online machining processes and achieving high machining accuracy [8]. Deyuan Ma and colleagues proposed a multi-sensor signal diagnostic approach for the online detection of critical porosity defects caused by pores in the laser welding process. The researchers utilized a multi-sensor platform to measure the three-dimensional morphological characteristics of critical pores during the welding process. They developed a method for identifying critical pore defect areas and extracting features for subsequent defect detection. The state of critical pores was monitored using a variety of sensing methods, including temperature measurement, high-speed camera imaging, glass plate imaging, X-ray imaging, and coherent light measurement. Deep learning technology, particularly Convolutional Neural Networks (CNN), was employed to process the acquired signals for detecting and locating pores caused by critical pores. The researchers conducted experiments and achieved satisfactory results, reaching an accuracy of 82.5% in pore detection. This method provides a real-time and accurate detection approach for porosity defects in the laser welding process [9]. Building upon these foundational studies, this paper aims to further explore the capabilities of OCT in laser welding quality

assessment. By integrating the latest advancements in AI and machine learning with OCT's high-resolution imaging, we propose a novel approach to address the current challenges in laser processing quality control. This research not only contributes to the existing body of knowledge but also opens new pathways for future innovations in laser processing technologies.

2 THE STRUCTURE AND WORKING PRINCIPLE OF OCT DETECTION SYSTEM

2.1 Experimental Setup

Fig. 1 shows the principle diagram of OCT detection system. It is mainly composed of light source system, optical fiber optical system, optical coherence imaging system, two-axis galvanometer two-dimensional scanning system, high-speed platform large-range detection system, diffraction optical system, image acquisition subsystem and computer. The light source system is SLED broadband light source with wavelength of 840 nm, which has the advantages of high output power and low wen-wave coefficient. Image acquisition subsystem is composed of linear array camera and image acquisition card. The mechanical motion subsystem consists of XY table, column, *Z*-axis moving parts, base, support base and servo motion system (servo motor, shaft encoder, motion control card). During measurement, the motion control system and grating ruler are used for accurate positioning, image data is obtained by the imaging system, and software is used for measurement.

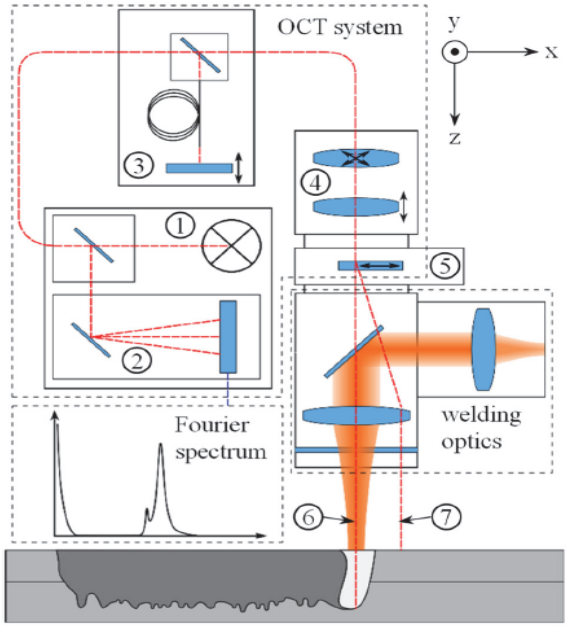

1. light source, 2. spectrometer, 3. reference arm, 4. collimation module, 5. beam splitter, 6.kehole measuring beam, 7.surface measuring beam

Figure 1 Optical concept of Fourier domain OCT [10]

2.2 Optical Concept of Fourier Domain OCT

The basic working principle of the system is the same as that of time-domain OCT, and the core components of frequency-domain OCT include three parts: light source, Michelson interference optical path and detector. The only difference is that the detector in the frequency domain OCT is replaced by the photodetector in the time domain OCT by a spectrograph to realize the signal measurement of the interference spectrum. After the light emitted from the light source passes through the fiber coupler, one beam enters the reference arm, is collimated by the lens to form parallel light incident on the reference plane mirror, is reflected by the plane mirror and returns along the original path to the fiber coupling through the lens, and the other beam incident on the scanning mirror after being collimated by the lens, is reflected by the focusing lens, and is incident on the sample. The incident light is backscattered from the sample and then coupled back into the fiber along the original path. The two beams of light are output through the output end of the fiber coupler, and incident on the diffraction grating after the collimation lens, and focus on the linear array CCD after the diffraction grating splitting to realize the detection of interference spectral signals. The electric fields returning from the reference E_R and the sample path E_S can be calculated as follows:

$$E_R = A_R \exp\left[-j\left(2\beta_R l_R - \omega t\right)\right] \tag{1}$$

$$E_S = A_S \exp\left[-j\left(2\beta_S l_S - \omega t\right)\right] \tag{2}$$

where ω is the optical frequency of the light source and β is the propagation constant. The factors of 2 multiplying the propagation constants β_R and β_S arise from the round-trip propagation of light to and from the reference and sample mirrors. The intensity of OCT interference signal can be calculated as follows:

$$I = \left\{\frac{\eta e}{h\nu}\left(\frac{\left|E_R + E_S\right|}{2\eta_0}\right)\right\} \tag{3}$$

where η is the detector quantum efficiency, e is the electronic charge, $h\nu$ is the photon energy, and η_0 is the intrinsic impedance of free space.

$$I = \frac{\eta e}{h\nu}\left(\frac{1}{\eta_0}\right)\left[\frac{1}{2}\left|A_R\right|^2 + \frac{1}{2}\left|A_S\right|^2 + real\left\{E_S E_R^*\right\}\right] \tag{4}$$

where the term:

$$real\left\{E_S E_R^*\right\} = A_R A_S \cos\left(2\beta_R l_R - 2\beta_S l_S\right) \tag{5}$$

describes the variation of the photocurrent with the positions of the reference and sample mirrors, in free space, the propagation constants are equal for the reference and sample fields, giving:

$$\beta_R = \beta_S = 2\pi/\lambda \tag{6}$$

and:

$$real\left\{E_S E_R^*\right\} = A_R A_S \cos\left(2\pi \frac{\Delta l}{\lambda/2}\right) \tag{7}$$

where $\Delta l = l_S - l_R$ is the mismatch in distance between the reference and sample beam paths. Eq. (5) shows that the photocurrent contains a sinusoidally varying term representing the interference between the reference and sample fields. The interference has a period of $\lambda/2$ relative to the length mismatch Δl. In developing a Frequency Domain Optical Coherence Tomography (FD-OCT) system for laser welding seam quality inspection, the key lies in accurately simulating the interference signal to fully consider the unique optical properties of the weld and welding materials. This precision is crucial for detecting minute defects and irregularities, as they directly impact the integrity and performance of the welded structure. The precise expression of the interference signal $I(k)$ takes into account the differences in optical properties between the weld and welding materials. This can be described by the following equation:

$$I(k) = S(k)\left[1 + \int_{-\infty}^{+\infty} R(z, k)\, \mathrm{e}^{i(2kz + \phi(z,k))}\mathrm{d}z\right]$$

Here, $S(k)$ represents the spectral intensity of the light source, while $R(z, k)$ and $\phi(z, k)$ denote the reflectivity and phase delay at depth z and wavenumber k, respectively, both of which may vary with the differences in the weld and welding materials. Because all of the interference information is contained in the case of low coherence light source will focus on calculating this term only.

3 THE KEY ALGORITHM OF OCT DETECTION SYSTEM

3.1 Hardware Algorithm

In order to increase the measurement speed and accuracy of the detection system, it is required that the system can process massive data in real time. In this paper, Nvidia's Compute Unified Device Architecture (CUDA) parallel computing architecture is adopted to solve the complex image processing problem of OCT by GPU. NVIDIA Compute Unified Device Architecture. NVIDIA released a parallel computing platform and programming model named CUDA to leverage the power of GPUs for enhanced computing performance. Data is prepared for processing in the host memory space by the CPU, transferred to the GPU memory space for CUDA processing and transferred back to the host memory space for output or display. The data stream into a PC acquired by a multi-functional spectral-domain OCT system can be substantial. Data streams can be upwards of 1 GB/sec for a top of the line PS-OCT-based spectrometer equipped with two 8 bit 1024 pixel spectrometers operating at 500 kHz. The data stream into a PC acquired by a multi-functional spectral-domain OCT system can be substantial. Data streams can be upwards of 1 GB/sec for a top of the line PS-OCT-based spectrometer equipped with two 8 bit 1024 pixel spectrometers operating at 500 kHz. Serialized code is executed on the CPU and parallelized code is executed on the GPU by calling C-based wrapper functions which invoke CUDA kernels. The collected data is prepared for processing by the CPU in the host memory space, then transmitted to the GPU space for CUDA processing, and finally returned to the host memory space for output and display.

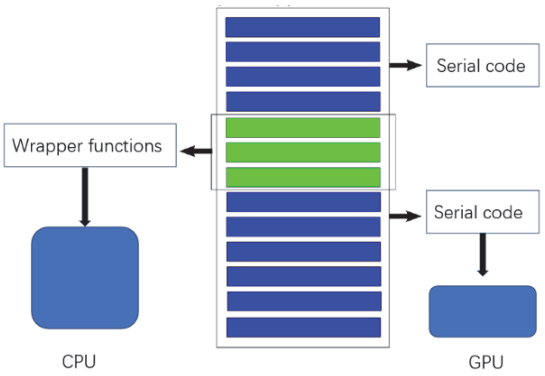

Figure 2 Hybrid CPU/GPU computing diagram

3.2 Deep Convolutional Neural Network Image Processing Algorithm [10]

With the emergence of advanced CUP and GPU and the continuous improvement of Convolution neural network algorithm, the use of convolution neural network algorithm to make OCT image feature extraction can effectively improve the efficiency and accuracy of image segmentation, and has self-adaptability. Firstly, the dual-number complex wavelet algorithm is used to denoise the image, and the OCT image background is preprocessed according to the double-tree complex wavelet algorithm. The processing results are shown in the figure below.

Figure 3 OCT image after noise reduction

Then, according to the deep convolutional neural network algorithm, different convolution kernels are used to extract the deep features of the image. The convolutional neural network model consists of the convolutional layer, activation layer, pooling layer, full link layer, etc. In this paper, based on the common defect types of aluminum alloy, the theoretical analysis of ResNet backpropagation and the adjustment of Residual Block structure, the convolutional neural network architecture as shown in the figure is built.

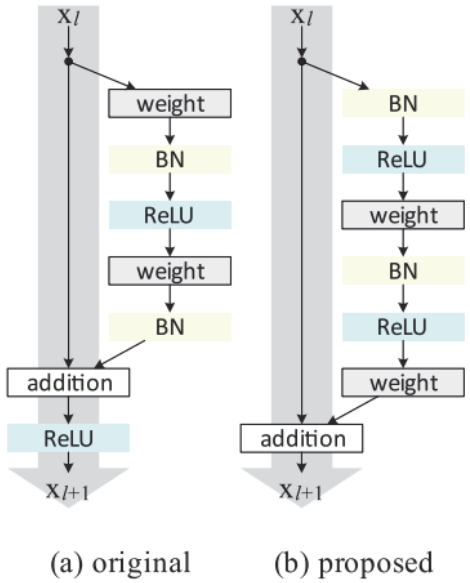

Figure 4 Deep convolutional neural network architecture diagram

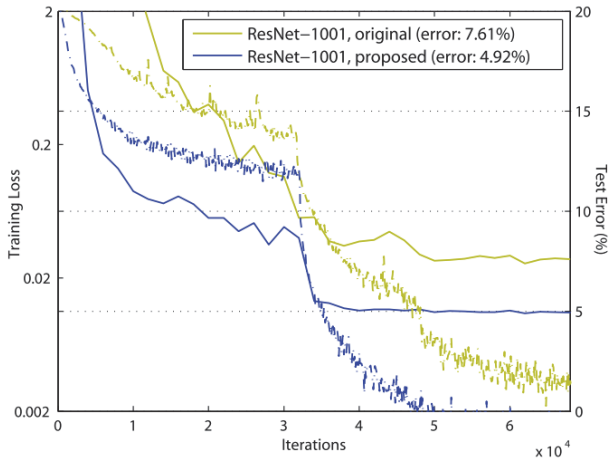

Figure 5 Original and proposed error

Deep residual networks (ResNets) consist of many stacked "Residual Units". Each unit can be expressed in a general form:

$$y_l = h(x_l) + F(x_l, w_l) \tag{8}$$

$$x_{l+1} = f(y_l) \tag{9}$$

where x_l and x_{l+1} are input and output of the lth unit, and F is a residual function. $h(x_l) = x_l$ is an identity mapping and f is a ReLU function.
If f is also an identity mapping: $x_{l+1} = y_l$, we can put Eq. (9) into Eq. (1) and obtain:

$$x_{l+1} = x_l + F(x_l, w_l) \tag{10}$$

Recursively:

$$\left(x_{l+2} = x_{l+1} + F(x_{l+1}, w_{l+1}) = \right.$$
$$\left. = x_l + F(x_l, w_l) + F(x_{l+1}, w_{l+1}), \text{ etc.}\right)$$

we will have:

$$x_L = x_l + \sum_{i=l}^{L-1} F(x_l, w_i) \tag{11}$$

Eq. (11) also leads to nice backward propagation properties. Denoting the loss function as E, from the chain rule of backpropagation we have

$$\frac{\partial \xi}{\partial x_l} = \frac{\partial \xi}{\partial x_L}\frac{\partial x_L}{\partial x_L} = \frac{\partial \xi}{\partial x_L}\left(1 + \frac{\partial}{\partial x_l}\sum_{i=l}^{L-1} F(x_i, w_i)\right) \tag{12}$$

4 MEASUREMENT EXPERIMENT AND RESULTS

4.1 Test of Laser Welding Quality Of Aluminum Alloy

The laser welded aluminum alloy workpieces were tested by OCT detector. The test workpiece is shown in the figure. The OCT system is installed on the laser welding device to achieve coaxial measurement optical path and laser welding optical path. Adjust the laser power, set to 4 kW, welding velocity 80 mm/s, welding and testing of aluminum alloy workpieces.

Figure 6 Al alloy laser welding workpiece

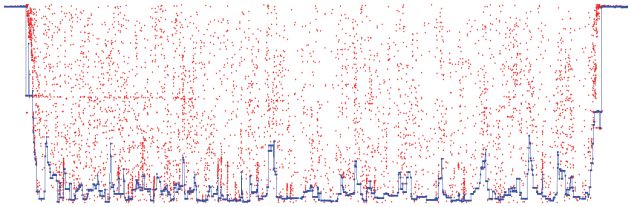

Figure 7 Welding depth of aluminum alloy workpiece

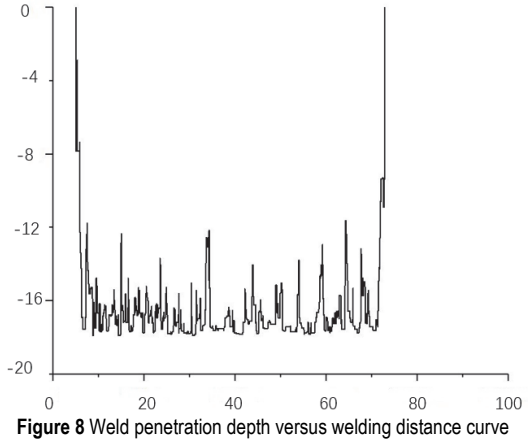

Figure 8 Weld penetration depth versus welding distance curve

Fig. 7 shows the real-time data collected by OCT for aluminum alloy welding. Fig. 8 is the curve of weld penetration depth versus welding distance. The detection data of weld length and welding depth are shown in the figure. Through the comparative analysis of failure test, it can be seen that the measurement accuracy of welding depth is better than 20 μm.

4.2 Defect Detection on the Weld Seam

In view of the laser welding quality detection technology, a large number of scholars have carried out in-depth research. Deyuan Ma et al. designed a real-time monitoring method for laser welding pores to measure the three-dimensional morphology of keyholes. A multi-sensor signal detection platform consisting of high-speed camera and optical coherence imaging is established [11]. Christian Stadter et al. used optical coherence tomography to measure the penetration of the welding process, and used copper and galvanized steel for welding tests [12]. However, how to measure the porosity defects in welds is a difficult problem in current research. Masanori Miyagi et al. used X-ray imaging to observe the dynamic formation process of laser welding holes. The keyhole and melt pool phenomena were observed by X-ray and a high speed video camera observation system. Predict the formation mechanism of keyhole. Youngseop Kim et al. performed laser processing on an ABS plastic as the total irradiation energy was varied. In the evaluation of the results of laser processing, we utilized a conventional SEM imaging method and the optical imaging method OCT [13, 14]. Meiko Boley et al. proposed a method to reliably extract the welding depth from OCT measurements recorded during laser welding. It was found that the noise can be separated from the significant measurements by analyzing the frequency of measurements in a given depth interval [7]. These methods fully verify that OCT technology can be applied in the field of laser welding quality inspection. In this paper, OCT detection technology is used to realize real-time and high-precision quality detection of aluminum alloy laser welding parts, and real-time adjustment of laser welding parameters can be achieved to achieve closed-loop control and improve welding quality.

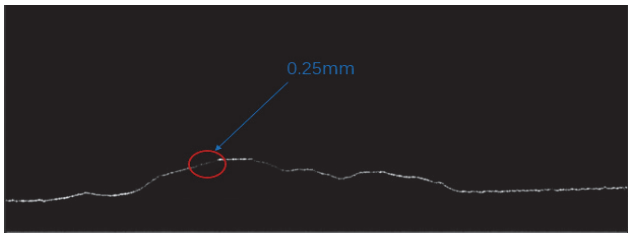

Figure 9 The figure of 0.25 mm welding porosity

For large-scale laser welding seam inspection, manual and visual inspection cannot meet the increasing quality standards, the deep convolutional neural network algorithm proposed in this study can be applied to optical coherence tomography inspection system. The experimental results show that the deep convolutional neural network algorithm has strong anti-interference ability. The image compression and noise reduction of weld penetration improve the detection accuracy. It can be seen from Fig. 9 that there is porosity with a diameter of 0.25 mm in the weld. Fig. 10 shows the measurement results of weld quality based on OCT principle. It can be seen from the measurement results that there is porosity with a diameter of 0.33 mm.

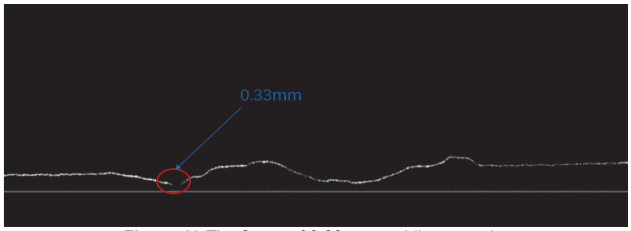

Figure 10 The figure of 0.33 mm welding porosity

5 CONCLUSIONS

In this study, we have addressed the critical need for on-line inspection of laser welding seam quality by proposing and implementing an innovative Optical Coherence Tomography (OCT) method for welding seam measurement. Our comprehensive exposition of the online OCT measurement system's structure and operational principles represents a significant leap in welding inspection technology. We have meticulously developed and analyzed a surface defect measurement algorithm using OCT, integrated with a sophisticated image processing algorithm based on a deep convolutional network. This integration marks a notable advancement in the field of welding quality assessment. The experimental application of this system to the laser welding of aluminum alloys has yielded results of paramount importance. We have demonstrated that our detection system achieves measurement accuracy at the micron level, a testament to the precision and efficacy of the OCT-based approach. Furthermore, our system has successfully accomplished the detection of weld penetration, a critical metric in evaluating the integrity and quality of laser welding seams. This achievement not only fulfills but also has the potential to surpass the existing standards for laser welding weld measurement. The implications of our findings extend far beyond the immediate application to aluminum alloys. This research contributes significantly to the broader field of materials engineering and manufacturing, offering a reliable, non-invasive solution for real-time quality assessment in industrial settings. The precision and adaptability of our OCT-based system pave the way for its application in a wider range of materials and welding contexts. Future research, building upon our findings, could explore the integration of this technology in automated manufacturing processes and its adaptation to various welding scenarios, further enhancing the efficiency and quality of welding practices.

Acknowledgment

This research was supported by Science and Technology Development Plan of Jilin Province. (No.20220508145RC).

6 REFERENCES

[1] Murta, R. H. F., Vieira, F. D. A., Santos, V. O., & de Moura, E. P. (2018). Welding Defect Classification from Simulated

Ultrasonic Signals. *Journal of Nondestructive Evaluation*, *37*. https://doi.org/10.1007/s10921-018-0496-y

[2] Zhang, K., Zhou, Z., & Zhou, J. (2015). Application of laser ultrasonic method for on-line monitoring of friction stir spot welding process. *Applied Optics*, *54*(25), 7483-7489. https://doi.org/10.1364/AO.54.007483

[3] Xu, H., Li, Y., & Jiang, C. (2018). Quantitative ultrasonic detection and tensile-shear property prediction for laser welds of stainless steel. *International Journal of Advanced Manufacturing Technology*, *99*, 301-311. https://doi.org/10.1007/s00170-018-2479-7

[4] He, K., Xiao, S., & Li, X. (2019). Time-frequency characteristics of acoustic emission signal for monitoring of welding structural state using Stockwell transform. *The Journal of the Acoustical Society of America*, *145*(1), 469. https://doi.org/10.1121/1.5087696

[5] Mayr, A., Lutz, B., Weigelt, M., Tobias, G., Dominik, K., Michael, M., Andreas, R., & Jörg, F. (2018). Evaluation of Machine Learning for Quality Monitoring of Laser Welding Using the Example of the Contacting of Hairpin Windings. *8th International Electric Drives Production Conference (EDPC)*. Schweinfurt, Germany, 1-7. https://doi.org/10.1109/EDPC.2018.8658346

[6] Schaumberger, K., Beck, M., & Saffer, J., Kaufmann, F., Ermer, J., Roth, S., & Schmidt, M. (2019). Improving process reliability by means of detection of weld seam irregularities in copper via thermographic process monitoring. *Procedia Manufacturing*, *36*, 58-63. https://doi.org/10.1016/j.promfg.2019.08.009

[7] Boley, M., Fetzer, F., Weber, R., & Thomas, G. (2019). High-speed x-ray imaging system for the investigation of laser welding processes. Journal of Laser App*lications*, *31*(4), 1-11. https://doi.org/10.2351/1.5110595

[8] Schmoeller, M., Weiss, T., Goetz, K., Stadter, C., Bernauer, C., & Zaeh, M. F. (2022). Inline Weld Depth Evaluation and Control Based on OCT Keyhole Depth Measurement and Fuzzy Control. *Processes*, *10*, 1422. https://doi.org/10.3390/pr10071422

[9] Ma, D., Jiang, P., Shu, L., & Geng, S. Identity Mappings in Deep Residual Networks. *Lecture Notes in Artificial Intelligence.*

[10] He, K. M., Zhang, X. Y., Ren, S. Q., et al. (2016). Identity Mappings in Deep Residual Networks. *Lecture Notes in Artificial Intelligence*, *9908*(2), 630-645.

[11] Ma, D., Jiang, P., Shu, L., & Shaoning, G. (2022). Real-time porosity monitoring during laser welding of aluminum alloys. *Journal of Manufacturing Systems*, *65*(10), 70-87. https://doi.org/10.1016/j.jmsy.2022.08.011

[12] Stadter, C., Schmoeller, M., von Rhein, L., & Zaeh, M. F. (2020). Real-time prediction of quality characteristics in laser beam welding using optical coherence tomography and machine learning. *Journal of Laser Applications*, *32*(5), 1-10. https://doi.org/10.2351/7.0000077

[13] Rahimi, M. & Parvareh, A. (2022). Real-time porosity monitoring during laser welding of aluminum alloys based on keyhole 3D morphology characteristics. *Journal of Manufacturing Systems*, *65*(10), 70-87. https://doi.org/10.1016/j.jmsy.2022.08.011

[14] Matsunawa, A., Seto, N., & Kim, J. D., et al. (2001). Observation of keyhole and molten pool behaviour in high power laser welding: mechanism of porosity formation and its suppression method. *Transactions of JWRI*, *30*(1), 13-27.

Contact information:

Zhengying JIANG
College of computer science and technology,
Changchun university of science and technology,
Changchun ,130022, China
College of Physics,
Changchun Normal University,
Changchun,130032, China

Zhengang JIANG
(Corresponding author)
College of computer science and technology,
Changchun university of science and technology,
Changchun ,130022, China
E-mail: 496240072@qq.com